Composite Structures 299 (2022) 116013

Contents lists available at ScienceDirect

Composite Structures

journal homepage: www.elsevier.com/locate/compstruct

# Moderately large vibrations of flexibly bonded layered beams with initial imperfections

Christoph Adam *, Dominik Ladurner, Thomas Furtmüller

*Unit of Applied Mechanics, University of Innsbruck, Technikerstr. 13, 6020 Innsbruck, Austria*

ARTICLE INFO

*Keywords:*
Imperfect beam
Interlayer slip
Layered beam
Nonlinear flexural vibrations
Slightly curved beam

ABSTRACT

In this paper, a beam theory is presented that allows to compute the moderately large dynamic response of slightly curved linear elastic layered beams with interlayer slip. The considered structural members are immovably supported, which leads to non-negligible membrane stresses at moderately large bending vibrations, and consequently to a geometrically nonlinear response. Based on a layerwise application of the Euler–Bernoulli theory, the boundary value problem is formulated for an arbitrary number of layers. A specification is then made for two- and three-layer beams. Several examples show the effect of an imperfect beam axis on the nonlinear dynamic response. A comparison of selected results with those of a much more expensive finite element analysis based on a plane stress state demonstrates the accuracy of the beam theory proposed.

## 1. Introduction

Structural members composed of several layers are used in numerous technical fields. The bonding of these layers is achieved by adhesives, nails, bolts, etc. Depending on the type of fastener, this connection may be flexible, which makes the mechanical behavior of these members under load more complex than of homogeneous components or layered components with rigid bond. In particular, the flexible bond causes a relative displacement of these layers, which is commonly referred to as interlayer slip. Examples of structural members with interlayer slip are components made of several glued or nailed wood layers, timber–concrete beams, composite steel–concrete bridges, components made of glued glass layers, small-scale composite parts in mechanical and aerospace engineering without complete bonding, etc.

In recent decades, numerous theories have been developed to predict the mechanical response of members with interlayer slip analytically or numerically with sufficient accuracy. From the early days, an example is the study [1] dedicated to the static response of flexibly bonded layered beams. Fundamental studies on the static response of linear elastic beams with flexible bond are summarized in papers [2,3]. In [4], the analytical solution of two-layer beams with interlayer slip based on two-dimensional elasticity is achieved. Steel–concrete beams with interlayer slip were recently investigated in [5]. A study on the response of curved beams with interlayer slip can be found in [6]. In a number of publications, the effect of second-order theory on the static response of these beams is presented, such as in [7,8]. The geometrically exact post-buckling response of layered columns with interlayer slip is analyzed in [9]. [10] provides a model that captures the time-dependent behavior of steel–concrete beams with partial interaction due to shrinkage and creep. In some cases, the fasteners behave nonlinearly, which is computationally captured, for example, in the papers [11,12]. Analytical solutions for three-layer beams with as stepwise linear interface law are found in [13].

Girhammar and Pan [14] were among the first to address the bending vibrations of elastic beams with interlayer slip. These studies were continued in further papers such as [15–17]. Challanel et al. [18] investigated the out-of-plane vibrations of layered beams with interlayer slip and general boundary conditions. In [19] the free vibrations of two-layer Timoshenko beams with interlayer slip are analyzed. In [20] it was shown how discontinuities such as elastic supports or rotational springs between the beam elements can be taken into account when predicting the dynamic response of layered beams with flexible bond. It should be noted here that delamination of layered structures is not captured with these theories. This topic is addressed, for example, in [21].

The geometrically nonlinear response of flexibly bonded layered beams at large deformations is addressed in [22–25]. When the supports of a structural member are fully restrained, geometric nonlinearities occur even at moderately large deformations, which significantly affect the response, shown for instance in [26]. For those structural members, even very small deviations from the straight beam axis have a large effect on the nonlinear response. This has been studied in detail for homogeneous beams or for layered beams with rigid bond, e.g. [27–29]. However, for beams with interlayer slip, a comprehensive

* Corresponding author.
*E-mail address:* christoph.adam@uibk.ac.at (C. Adam).

https://doi.org/10.1016/j.compstruct.2022.116013
Received 28 February 2022; Received in revised form 3 June 2022; Accepted 28 July 2022
Available online 6 August 2022

treatment of an imperfect beam axis on the response is lacking. As a starting point, a beam theory for slightly curved symmetrically layered beams with interlayer slip subjected to static loads was recently derived in [30]. Under dynamic excitation, however, these investigations are still waiting.

In the present paper, therefore, a beam theory for predicting the moderately large vibration response of linear elastic beams with interlayer slip is presented. These beams can be composed of any number of layers. A basis for this beam theory are two recent publications which treat the static [31] and dynamic [32] behavior of symmetrically layered three-layer beams with interlayer slip and perfectly straight beam axis on fully immovable supports. It is assumed that the shear deformations of the individual layers are negligible, and consequently, the Euler–Bernoulli theory can be applied layerwise. The nonlinear strain of the beam axis is taken into account according to a theory by Mettler [33]. After deriving the equations of motion and the applicable boundary conditions, these equations are specified for two special configurations, namely the asymmetrically layered two-layer beam and the symmetrically layered three-layer beam. The validation of the proposed theory is performed by comparative numerical computations on several beams based on a plane stress state, which are however much more computationally demanding. In several application examples, the grave effect of small geometric imperfections on the dynamic response is demonstrated.

## 2. Basic equations

Consider a single-span beam composed of an arbitrary number of $n$ elastically bonded layers. Each layer is homogeneous and has a cross-section that is symmetrical about the vertical axis and constant over the span length $l$. The centers of gravity of the layers are on top of each other. The top layer and its parameters are denoted by the subscript "1", the numbering of the layers below is successively increasing from top to bottom, as shown in Fig. 1 for a four-layer beam as an example. The material of the $i$th layer ($i = 1,\dots,n$) is characterized by the Young's modulus $E_i$ and the mass density $\rho_i$. The $n-1$ interfaces between the layers and their parameters are also denoted by the subscript $i$, with $i = 1$ for the interface between the first and second layer, and $i = n-1$ for the interface between the second last and the bottom layer. The slip modulus at the $i$th interface denoted by $K_{si}$ represents the longitudinal flexibility of the layer bonding.

The beam axis is defined by the line connecting the elastic centers of gravity of the complete cross-section of the beam with rigidly bonded layers. In the stress-free state, this beam axis has a small initial deflection $\hat{w}$ that varies over the beam length, which either represents an imperfection of a straight beam or may be intentional. The deformations of the beam are referred to a Cartesian $x, y, z$-coordinate system with the origin in the beam axis at the left end of the beam and coordinate orientation according to Fig. 1. The lateral coordinate $\zeta_i$ is specified layerwise, with the pre-curved neutral axis of the $i$th layer serving as origin ($\zeta_i = 0$), see also Fig. 1. The vertical time-varying line load $p(x,t)$ applied in the beam axis excites the structural member to vibrations in the $xz$-plane.

Since the layers are elastically connected, the layers translate relative to each other under load in longitudinal direction, which is referred to as interlayer slip. Subsequently, the interlayer slip between the $i$th and the $(i+1)$-th layer is denoted as $\Delta u_i(x,t)$. Furthermore, it is assumed that the layers are rigid in shear. Therefore, the Euler–Bernoulli theory can be applied separately for each layer. At time $t$, the displacement field shown in Fig. 2 as an example of a four-layer beam can accordingly be expressed as follows,

$$w_i(x,t) = w(x,t)\,,\;\; u_i(x,\zeta_i,t) = u_i^{(0)}(x,t) - \zeta_i w_{,x}(x,t) \qquad i = 1,\dots,n \tag{1}$$

The variable $w(x,t)$ denotes the deflection, which at a position $x$ is the same for all layers and fibers. The deflection $w(x,t)$ is superposed to the initial imperfection $\hat{w}(x)$. $u_i(x,\zeta_i,t)$ represents the longitudinal displacement of the fiber at the vertical distance $\zeta_i$ from the center of gravity of the cross-section of the $i$th layer. The axial displacement at $\zeta_i = 0$ is denoted as $u_i^{(0)}(x,t)$, compare with Fig. 2. $(.)_{,x}$ indicates the partial derivative of $(.)$ with respect to coordinate $x$.

The layerwise axial displacements below the top layer $u_i^{(0)}(x,t)$, $i = 2,\dots,n$, can be expressed as a function of the axial displacement of the top layer, $u_1^{(0)}(x,t)$, the cross-sectional rotation $w_{,x}(x,t)$ and the sum of the interlayer slips above the $i$th layer, compare with Fig. 2,

$$u_i^{(0)}(x,t) = u_1^{(0)}(x,t) - (d+z_i)w_{,x}(x,t) + \sum_{j=1}^{i-1} \Delta u_j(x,t)\,,\;\; i = 2,\dots,n \tag{2}$$

where $z_i$ is the vertical coordinate from the beam axis to the center of gravity of the $i$th layer, and $d$ denotes the distance from the center of gravity of the top layer to the elastic center of gravity of the beam. Assuming that the beam axis is located in the $m$th layer, the axial displacement of the top layer $u_1^{(0)}(x,t)$ can be expressed by the axial displacement of the beam axis $u^{(\infty)}(x,t)$ as follows,

$$u^{(\infty)}(x,t) = u_1^{(0)}(x,t) - w_{,x}(x,t)d + \sum_{j=1}^{m-1} \Delta u_j(x,t) \tag{3}$$

and further

$$u_1^{(0)}(x,t) = u^{(\infty)}(x,t) + w_{,x}(x,t)d - \sum_{j=1}^{m-1} \Delta u_j(x,t) \tag{4}$$

A moderately large deflection $w(x,t)$ leads to a nonlinear axial strain–displacement relation (see e.g. [34]). For a layered beam with the initial imperfection $\hat{w}(x)$, according to [33] the strain in the longitudinal axis of $i$th layer reads as

$$e_i(x,t) = u_{i,x}^{(0)}(x,t) + \frac{1}{2}w_{,x}^2(x,t) + w_{,x}(x,t)\hat{w}_{,x}(x)\,, \qquad i = 1,\dots,n \tag{5}$$

The longitudinal strain of any fiber at distance $\zeta_i$ from the center of gravity of the $i$th layer is therefore

$$\epsilon_i(x,\zeta_i,t) = e_i(x,t) - \zeta_i w_{,xx}(x,t) = u_{i,x}^{(0)}(x,t) + \frac{1}{2}w_{,x}^2(x,t) + w_{,x}(x,t)\hat{w}_{,x}(x) - \zeta_i w_{,xx}(x,t)\,, \quad i = 1,\dots,n \tag{6}$$

It is moreover assumed that the stresses are in the linear elastic range and thus Hooke's law applies. Multiplying the strain $\epsilon_i(x,\zeta_i,t)$ by the Young's modulus $E_i$ of the $i$th layer leads to the longitudinal stresses in this layer. Then, the axial forces $N_i$ in the individual layers are obtained by integrating these stresses layer by layer in combination with Eqs. (5), (2) and (4) as follows,

$$\begin{aligned} N_i &= E_i A_i e_i = E_i A_i \left(u_{i,x}^{(0)} + \frac{1}{2}w_{,x}^2 + w_{,x}\hat{w}_{,x}\right) \\ &= E_i A_i \left(u_{,x}^{(\infty)} - z_i w_{,xx} + \frac{1}{2}w_{,x}^2 + w_{,x}\hat{w}_{,x} + \sum_{j=1}^{i-1}\Delta u_{j,x} - \sum_{j=1}^{m-1}\Delta u_{j,x}\right), \\ &\quad i = 1,\dots,n \end{aligned} \tag{7}$$

with the axial stiffness $E_i A_i$ and the cross-sectional area of the $i$th layer. Accordingly, integration of the longitudinal stresses multiplied by $\zeta_i$ over the $i$-the cross-sectional area yields the layerwise bending moment [34]

$$M_i = -E_i J_i w_{,xx}\,, \qquad i = 1,\dots,n \tag{8}$$

where $E_i J_i$ is the bending stiffness and $J_i$ the area moment of inertia about the $\eta_i$-axis of the $i$th layer (compare with Fig. 1).

The interlaminar shear traction between the $i$th and the $(i+1)$-th layer $t_{si}$ is assumed to be proportional to the corresponding interlayer slip $\Delta u_i$,

$$t_{si} = K_{si}\Delta u_i\,, \qquad i = 1,\dots,n-1 \tag{9}$$

Once the kinematic relations and stress resultants have been established, the next step is to apply at time $t$ conservation of momentum to

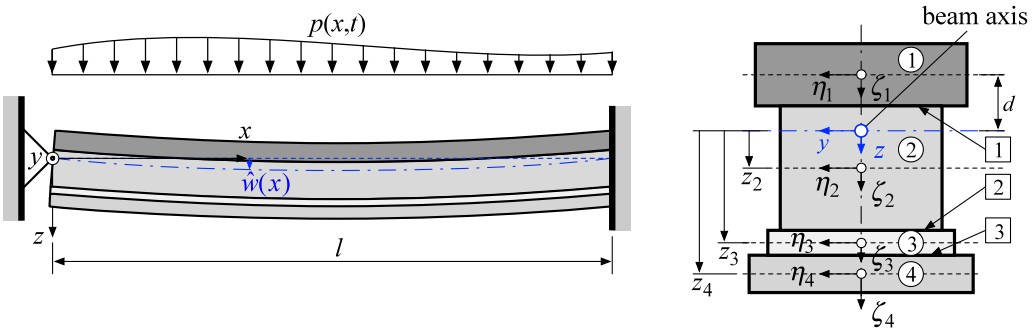


**Fig. 1.** Immovably supported imperfect beam composed of four elastically bonded layers.

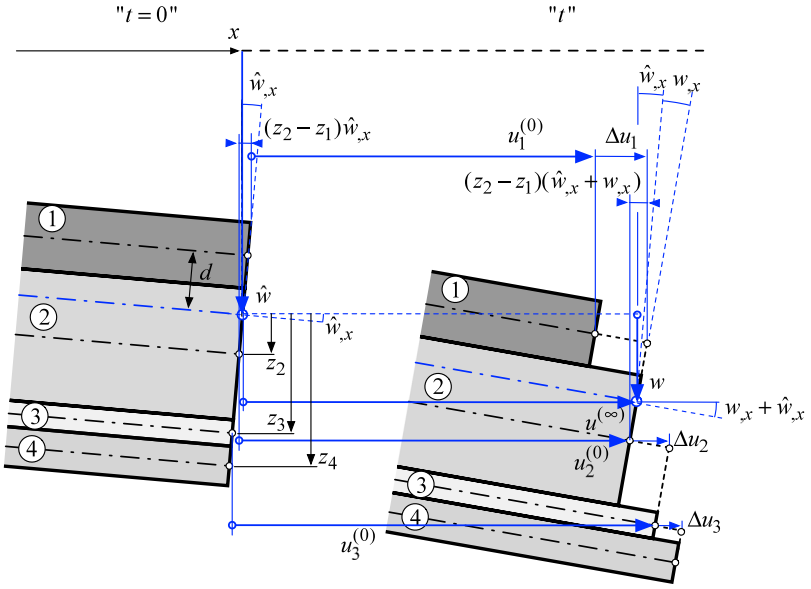


**Fig. 2.** Cross-section of a four-layer beam at $x$ in its initial (time $t = 0$) and its deformed state (time $t$).

an infinitesimally small beam element in its deformed state as shown in Fig. 3, to capture the effects of second order. In doing so, it is assumed that the horizontal as well as the rotational inertia are very small compared to the vertical inertia, and are thus neglected.

Consequently, the resulting beam theory yields reasonable results only in the lower frequency range. The layerwise application of conservation of momentum in the $x$-direction therefore degenerates to the following equilibrium conditions,

$$N_{i,x} + t_{si} - t_{si-1} = 0\,, \qquad i = 1, \dots, n\,, \qquad t_{s0} = 0\,,\ t_{sn} = 0 \tag{10}$$

As common in second order analysis, instead of the horizontal forces $S_i$, $i = 1, \dots, n$, the corresponding layerwise axial forces $N_i$, $i = 1, \dots, n$, have been used. Eqs. (10) represent the relation between the layerwise axial forces and the shear tractions. Summing up these $n$ equations, provides the equilibrium condition for the normal force $N$ in the entire cross-section, compare with Fig. 3,

$$N_{,x} = 0 \tag{11}$$

with

$$N = \sum_{i=1}^{n} N_i \tag{12}$$

The relationship Eq. (11) is equally found from the equilibrium of the entire beam element in $x$-direction. It reveals that $N$ is constant along the span $l$ but a function of the time $t$, i.e. $N(t)$. Since the external load in the $x$-direction is zero, the normal force $N$ results from the strain in the beam axis due to moderately large bending vibrations.

Conservation of momentum in vertical ($z$-)direction results in the following differential equation,

$$T_{,x} + p = \mu \ddot{w} \tag{13}$$

with $T$ denoting the transverse cross-sectional force and $\mu = \sum_{i=1}^{n} \rho_i A_i$ the mass per unit length. $\dot{(\cdot)}$ indicates the partial derivative of $(\cdot)$ with respect to time $t$, and thus $\ddot{w}$ is the transverse acceleration. Next, conservation of momentum about the $y$-axis is applied to the infinitesimal beam element in its deformed state, which gives

$$M_{,x} + N\left(w_{,x} + \hat{w}_{,x}\right) - T = 0 \tag{14}$$

because the rotational inertia has been omitted, as discussed above. The overall bending moment $M$ is determined from the layerwise stress resultants according to

$$M = \sum_{i=1}^{n} \left(M_i + N_i z_i\right) \tag{15}$$

Finally, the two equations Eqs. (13) and (14) are transformed into a single equation by differentiating Eq. (14) with respect to $x$ and then inserting it into equation Eq. (13),

$$\mu \ddot{w} - M_{,xx} - N\left(w_{,xx} + \hat{w}_{,xx}\right) = p \tag{16}$$

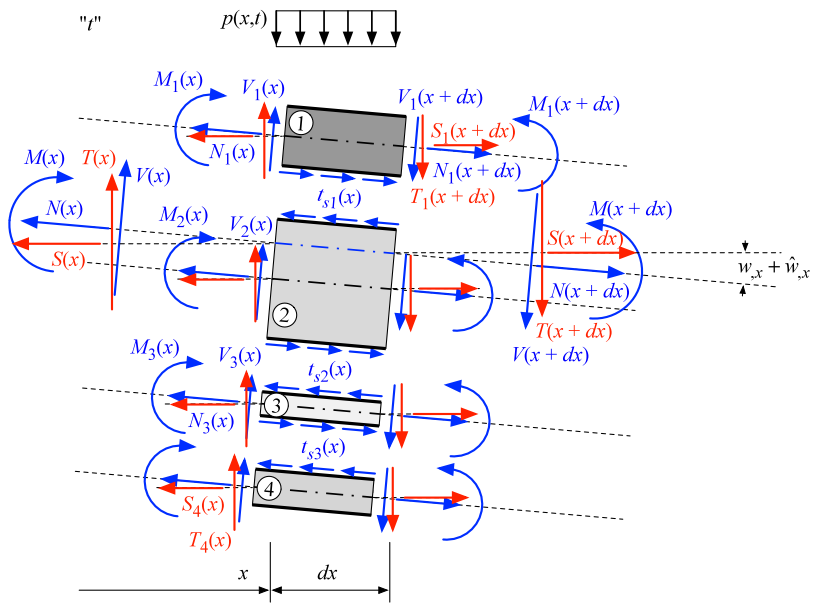


**Fig. 3.** Free-body diagram of a deformed infinitesimal four-layer beam element at time $t$. First order (in red) and second order (in blue) internal forces.

## 3. Boundary value problem

### 3.1. Equations of motion

The response of the beam under consideration is fully determined when the deflection $w$, the interlayer slips $\Delta u_i$, $i = 1, \dots, n-1$, as well as the longitudinal displacement $u^{(\infty)}$ and their spatial and temporal derivatives are known. The boundary value problem for the beam problem at hand must therefore be formulated with these kinematic variables. The basis for the first set of solution equations are the equilibrium conditions Eq. (10), in which the shear tractions $t_{si}$ are replaced by Eq. (9) and the layerwise normal forces $N_i$ by Eq. (7). This leads to the following $n$ relationships,

$$E_i A_i \Big( u^{(\infty)}_{,xx} - z_i w_{,xxx} + w_{,x} w_{,xx} + w_{,x} \hat{w}_{,xx} + w_{,xx} \hat{w}_{,x} + \sum_{j=1}^{i-1} \Delta u_{j,xx} - \sum_{j=1}^{m-1} \Delta u_{j,xx} \Big) + K_{si} \Delta u_i - K_{si-1} \Delta u_{i-1} = 0\,, \qquad i = 1, \dots, n\,, \qquad \Delta u_0 = 0\,,\ \Delta u_n = 0 \tag{17}$$

Before the equation of motion can be established, the overall bending moment $M$ must be expressed as a function of the kinematic variables. This is achieved by substituting the layerwise cross-sectional forces according to Eqs. (7) and (8) into Eq. (15),

$$M(x,t) = -EJ_\infty w_{,xx} + \sum_{i=1}^{n} \Big( E_i A_i z_i \Big( \sum_{j=1}^{i-1} \Delta u_{j,x} - \sum_{j=1}^{m-1} \Delta u_{j,x} \Big) \Big) \tag{18}$$

with

$$EJ_\infty = EJ_0 + \sum_{i=1}^{n} E_i A_i z_i^2 \tag{19}$$

denoting the bending stiffness of the beam with rigidly bonded layers, and

$$EJ_0 = \sum_{i=1}^{n} E_i J_i \tag{20}$$

the bending stiffness of the member without bond, i.e. $K_{si} = 0$, $i = 1, \dots, n-1$. The bending moment presented in this manner is differentiated twice with respect to $x$ and then inserted into Eq. (16). This yields the equation of motion

$$\mu \ddot{w} + EJ_\infty w_{,xxxx} - \sum_{i=1}^{n} \Big( E_i A_i z_i \Big( \sum_{j=1}^{i-1} \Delta u_{j,xxx} - \sum_{j=1}^{m-1} \Delta u_{j,xxx} \Big) \Big) - N \left( w_{,xx} + \hat{w}_{,xx} \right) = p \tag{21}$$

The total normal force $N$ that appears in this equation is obtained by substituting the $n$ layerwise normal forces $N_i$, $i = 1, \dots, n$, according to Eq. (7) in Eq. (12),

$$N(t) = EA_e \Big( u^{(\infty)}_{,x} + \frac{1}{2} w^2_{,x} + w_{,x} \hat{w}_{,x} \Big) + \sum_{i=1}^{n} \Big( E_i A_i \Big( \sum_{j=1}^{i-1} \Delta u_{j,x} - \sum_{j=1}^{m-1} \Delta u_{j,x} \Big) \Big) \tag{22}$$

$$EA_e = \sum_{i=1}^{n} E_i A_i \tag{23}$$

Substituting $N$ in Eq. (11) by this expression yields another governing equation,

$$EA_e \Big( u^{(\infty)}_{,xx} + w_{,x} w_{,xx} + w_{,x} \hat{w}_{,xx} + w_{,xx} \hat{w}_{,x} \Big) + \sum_{i=1}^{n} \Big( E_i A_i \Big( \sum_{j=1}^{i-1} \Delta u_{j,xx} - \sum_{j=1}^{m-1} \Delta u_{j,xx} \Big) \Big) = 0 \tag{24}$$

which can be used as an alternative to one of the $n$ Eqs. (17).

### 3.2. Boundary conditions

The solution of the coupled Eqs. (17) and (21) is obtained with the boundary conditions that are provided below for three different types of supports. In particular, hinged supports without shear restraints (referred to as soft-hinged supports), hinged supports with shear restraints (referred to as hard-hinged supports) and rigidly clamped ends are taken into account. Free ends are not considered, as in this case no significant nonlinear membrane stresses develop in the member axis with moderately large bending vibrations. Consequently, in a member with a free end the geometrically linear and the geometrically nonlinear response are almost identical.

For the three support conditions considered, both the deflection and the horizontal displacement of the support point are constrained, i.e.

$$w_b = 0 \tag{25}$$

$$u^{(\infty)}_b = 0 \tag{26}$$

The subscript $b$ indicates a boundary point (i.e. $x = 0$ or $x = l$).

*Soft-hinged support.* For a hinged support the overall moment is zero, i.e. $M_b = 0$. According to Eq. (18), therefore, the following relationship between the kinematic variables results at the boundary,

$$\left(-EJ_\infty w_{,xx} + \sum_{i=1}^{n}\left(E_i A_i z_i\left(\sum_{j=1}^{i-1}\Delta u_{j,x} - \sum_{j=1}^{m-1}\Delta u_{j,x}\right)\right)\right)_b = 0 \tag{27}$$

Furthermore, at the boundary, the layerwise normal forces are zero with the exception of the $m$th layer in which the support is located,

$$(N_i)_b = 0\,, \quad i = 1,\dots,m-1,m+1,\dots,n\,, \tag{28}$$

and further

$$\left(u^{(\infty)}_{,x} - z_i w_{,xx} + \frac{1}{2}w^2_{,x} + w_{,x}\hat{w}_{,x} + \sum_{j=1}^{i-1}\Delta u_{j,x} - \sum_{j=1}^{m-1}\Delta u_{j,x}\right)_b = 0\,,$$
$$i = 1,\dots,m-1,m+1,\dots,n \tag{29}$$

In the $m$th layer, the overall normal force $N$, which corresponds to the horizontal support component, is imposed, and thus the normal force in this layer $N_m$ is equal to the overall normal force $N$,

$$(N_m)_b = N_b\,, \quad i = m \tag{30}$$

or

$$EA_e\left(u^{(\infty)}_{,x} + \frac{1}{2}w^2_{,x} + w_{,x}\hat{w}_{,x}\right)_b + \sum_{i=1}^{n}\left(E_i A_i\left(\sum_{j=1}^{i-1}\Delta u_{j,x} - \sum_{j=1}^{m-1}\Delta u_{j,x}\right)\right)_b$$
$$= E_m A_m\left(u^{(\infty)}_{,x} - z_m w_{,xx} + \frac{1}{2}w^2_{,x} + w_{,x}\hat{w}_{,x}\right)_b\,, \quad i = m \tag{31}$$

*Hard-hinged support.* With a hard-hinged end, the bending moment vanishes as with a soft-hinged support, thus the boundary condition Eq. (27) applies. Moreover, in a hard-hinged support, the interlayer slips are fully constrained by a rigid end plate,

$$(\Delta u_i)_b = 0\,, \quad i = 1,\dots,n-1 \tag{32}$$

At such a boundary, the shear tractions are therefore also zero, $(t_{si})_b = 0$, $i = 1,\dots,n-1$.

*Rigidly clamped end.* At a rigidly clamped end, the slope of the lateral deflection is zero,

$$(w_{,x})_b = 0 \tag{33}$$

Additionally, no interlayer slip can occur, which means that the boundary condition Eq. (32) is also valid here.

### 3.3. Three-layer beam with symmetric layer arrangement

In the following, the boundary value problem is specified for symmetrically layered beam consisting of three layers (i.e. $n = 3$), where both geometry and material parameters of the two face layers are identical, i.e. $E_1A_1 = E_3A_3$, $E_1J_1 = E_1J_3$, $\rho_1 = \rho_3$, $z_1 = -z_3$. The slip modulus of the two interfaces is also supposed to be the same. i.e. $K_{s1} = K_{s2}$. The beam axis thus coincides with the axis of the middle layer, i.e. $u^{(\infty)} = u_2^{(0)}$ and $m = 2$. The deformation is governed by the following four kinematic variables: $w$, $u^{(\infty)}$, $\Delta u_1$, $\Delta u_2$.

For this beam, the following three equations result from Eqs. (17),

$$E_1A_1\left(u^{(\infty)}_{,xx} - z_1 w_{,xxx} + w_{,x}w_{,xx} + w_{,x}\hat{w}_{,xx} + w_{,xx}\hat{w}_{,x} - \Delta u_{1,xx}\right) + K_{s1}\Delta u_1 = 0 \tag{34}$$

$$E_2A_2\left(u^{(\infty)}_{,xx} + w_{,x}w_{,xx} + w_{,x}\hat{w}_{,xx} + w_{,xx}\hat{w}_{,x}\right) + K_{s1}(\Delta u_2 - \Delta u_1) = 0 \tag{35}$$

$$E_1A_1\left(u^{(\infty)}_{,xx} + z_1 w_{,xxx} + w_{,x}w_{,xx} + w_{,x}\hat{w}_{,xx} + w_{,xx}\hat{w}_{,x} + \Delta u_{2,xx}\right) - K_{s1}\Delta u_2 = 0 \tag{36}$$

which couple all kinematic variables. Moreover, Eq. (24) becomes

$$EA_e\left(u^{(\infty)}_{,xx} + w_{,x}w_{,xx} + w_{,x}\hat{w}_{,xx} + w_{,xx}\hat{w}_{,x}\right) + E_1A_1(\Delta u_{2,xx} - \Delta u_{1,xx}) = 0 \tag{37}$$

In Eqs. (34)–(37) the four governing kinematic variables are coupled, which is disadvantageous for the solution. When, on the one hand, Eq. (36) is subtracted from Eq. (34) and, on the other hand, the two Eqs. (34) and (36) are added and Eq. (37) is used to eliminate the variables $u^{(\infty)}$, $w$ and $\hat{w}$, alternatively, two equations are obtained without $u^{(\infty)}$ and $\hat{w}$,

$$\Delta u_{2,xx} + \Delta u_{1,xx} - \frac{K_{s1}}{E_1A_1}(\Delta u_2 + \Delta u_1) + 2z_1 w_{,xxx} = 0 \tag{38}$$

$$\Delta u_{2,xx} - \Delta u_{1,xx} - \kappa^2(\Delta u_2 - \Delta u_1) = 0\,, \quad \kappa = \left(\frac{EA_eK_{s1}}{E_1A_1E_2A_2}\right)^{1/2} \tag{39}$$

The set of governing equations is completed by rewriting Eq. (21) for the three-layered beam,

$$\mu\ddot{w} + EJ_\infty w_{,xxxx} + E_1A_1z_1(\Delta u_{1,xxx} + \Delta u_{2,xxx}) - N\left(w_{,xx} + \hat{w}_{,xx}\right) = p \tag{40}$$

where

$$N(t) = \frac{EA_e}{l}\int_0^l\left(u^{(\infty)}_{,x} + \frac{1}{2}w^2_{,x} + w_{,x}\hat{w}_{,x}\right)dx - \frac{E_1A_1}{l}\int_0^l(\Delta u_{1,x} - \Delta u_{2,x})dx \tag{41}$$

Since the normal force is constant over the length $l$ (see Eq. (11)), the representation of the normal force in the form of an integral chosen above is more convenient for the solution of the boundary value problem, see e.g. [33] for dynamic buckling analysis of homogeneous beams.

Naturally, the two boundary conditions Eqs. (25) and (26) valid for all considered support conditions do not change when the number of layers is varied. However, due to the symmetrical layer arrangement, the boundary conditions according to Eqs. (27) and (29) simplify considerably for a soft-hinged support. Evaluating Eq. (29) for the first and third layer, subtracting one of the equations from the other, and substituting the resulting expression into Eq. (27), the following is obtained,

$$(w_{,xx})_b = 0 \tag{42}$$

and further

$$(\Delta u_{1,x} + \Delta u_{2,x})_b = 0 \tag{43}$$

The fifth boundary condition for a soft-hinged end according to Eq. (31) then becomes

$$(\Delta u_{2,x} - \Delta u_{1,x})_b + 2\left(u^{(\infty)}_{,x} + \frac{1}{2}w^2_{,x} + w_{,x}\hat{w}_{,x}\right)_b = 0 \tag{44}$$

With a hard-hinged support, according to Eq. (32)

$$(\Delta u_1)_b = (\Delta u_2)_b = 0 \tag{45}$$

The vanishing of the overall moment further requires that (see Eq. (27))

$$\left(-EJ_\infty w_{,xx} - E_1A_1z_1(\Delta u_{1,x} + \Delta u_{2,x})\right)_b = 0 \tag{46}$$

At a clamped end, the two boundary conditions Eq. (45) and the boundary condition Eq. (33) apply to the three-layer beam.

### 3.4. Two-layer beam

As a second important special case, an asymmetrically layered beam consisting of two layers is considered (i.e. $n = 2$). It is assumed that the beam axis is in the lower layer (i.e. $m = 2$). The governing kinematic variables are the deflection $w$, the longitudinal displacement $u^{(\infty)}$ and

the interlayer slip $\Delta u_1$. For this configuration, from Eqs. (17) follow two relations,

$$E_1A_1\left(u^{(\infty)}_{,xx} - z_1 w_{,xxx} + w_{,x}w_{,xx} + w_{,x}\hat{w}_{,xx} + w_{,xx}\hat{w}_{,x} - \Delta u_{1,xx}\right) + K_{s1}\Delta u_1 = 0 \tag{47}$$

$$E_2A_2\left(u^{(\infty)}_{,xx} - z_2 w_{,xxx} + w_{,x}w_{,xx} + w_{,x}\hat{w}_{,xx} + w_{,xx}\hat{w}_{,x}\right) - K_{s1}\Delta u_1 = 0 \tag{48}$$

When the first of these equations is divided by $E_1A_1$ and the second by $E_2A_2$, and then the second is subtracted from the first equation, the following simpler relationship is obtained,

$$\Delta u_{1,xx} - \kappa^2\Delta u_1 + (z_1 - z_2)w_{,xxx} = 0 \tag{49}$$

where neither the nonlinear terms nor the longitudinal displacement $u^{(\infty)}$ are included. In addition to this equation, Eq. (24) specified for this two-layer configuration is used to solve the boundary value problem,

$$EA_e\left(u^{(\infty)}_{,xx} + w_{,x}w_{,xx} + w_{,x}\hat{w}_{,xx} + w_{,xx}\hat{w}_{,x}\right) - E_1A_1\Delta u_{1,xx} = 0 \tag{50}$$

Rewriting Eq. (21) for the problem at hand finally provides the equation of motion,

$$\mu\ddot{w} + EJ_\infty w_{,xxxx} + E_1A_1z_1\Delta u_{1,xxx} - N\left(w_{,xx} + \hat{w}_{,xx}\right) = p \tag{51}$$

with

$$N(t) = EA_e\left(u^{(\infty)}_{,x} + \frac{1}{2}w^2_{,x} + w_{,x}\hat{w}_{,x}\right) - E_1A_1\Delta u_{1,x} \tag{52}$$

To solve this boundary value problem, four boundary conditions must be specified for each boundary. For all types of supports considered, these are the two boundary conditions $w_b = 0$ and $u^{(\infty)}_b = 0$ (see Eqs. (25) and (26)).

For a soft-hinged support, the two remaining boundary conditions originate from Eqs. (27) and (29),

$$\left(-EJ_\infty w_{,xx} - E_1A_1z_1\Delta u_{1,x}\right)_b = 0 \tag{53}$$

$$\left(u^{(\infty)}_{,x} - z_1w_{,xx} + \frac{1}{2}w^2_{,x} + w_{,x}\hat{w}_{,x} - \Delta u_{1,x}\right)_b = 0 \tag{54}$$

It should be noted that the boundary condition given in Eq. (31) degenerates to the boundary condition Eq. (54).

For a hard-hinged support, the boundary condition Eq. (53) also applies. The fourth boundary condition results from Eq. (32),

$$(\Delta u_1)_b = 0 \tag{55}$$

A clamped end requires the satisfaction of the two boundary conditions Eqs. (33) and (55).

## 4. Procedure of analysis

The Galerkin method [34] is used to solve the present boundary value problem. The deflection $w(x,t)$ is approximated by the Ritz approach

$$w(x,t) \approx w^*(x,t) = \sum_{i=1}^{J} Y_i(t)\Phi_i(x) \tag{56}$$

The $J$ shape functions $\Phi_i(x)$ must satisfy the kinematic boundary conditions in $w$ (i.e. Eqs. (25) and (33)), whereas the dynamic boundary conditions (i.e. Eqs. (53) (two-layer beam) and (46) (three-layer beam)) should be satisfied. In the case of a two-layer beam, the Ritz approach is inserted into Eqs. (49) and (50), which are then solved for $u^{(\infty)}$ and $\Delta u_1$ as a function of the unknown $Y_i(t)$ with the boundary conditions Eqs. (53) and (54) (soft-hinged end), and Eqs. (53) and (55) (hard-hinged end and clamped end), respectively.

For the three-layer beam, the corresponding governing equations Eqs. (38), (39) and (37) with the boundary conditions Eqs. (26), (43), (44) (soft-hinged end), and (26) and (45) (hard-hinged end and clamped end), respectively, are solved for $u^{(\infty)}$, $\Delta u_1$ and $\Delta u_2$.

These variables are inserted into the expression for the normal force $N(t)$, which thus also becomes a function of $Y_i(t)$, $i = 1,\dots,J$. Then $N(t)$, as well as the corresponding derivatives with respect to $x$ of $w$ and $\Delta u_1$ (and $\Delta u_2$) are inserted into the equation of motion Eq. (51) (two-layer beam) or Eq. (40) (three-layer beam), respectively. This equation is successively multiplied by the shape functions $\Phi_i$, $i = 1,\dots,J$, according to the Galerkin method [34] and integrated over the span $l$. In the case that the shape functions do not satisfy the dynamic boundary conditions, the resulting work of the boundary forces is to be added [34],

$$\int_0^l \left(\mu\ddot{w}^* + EJ_\infty w^*_{,xxxx} + E_1A_1z_1\Delta u^*_{1,xxx} - N^*\left(w^*_{,xx} + \hat{w}_{,xx}\right) - p\right)\Phi_i dx - M^*_b(\Phi_{i,x})_b + T^*_b(\Phi_i)_b = 0,$$
$$i = 1,\dots,J \tag{57}$$

given here as an example for the two-layer beam. The superscript $*$ denotes the quantities based on the Ritz approximation Eq. (56). By partial integrating these equations twice with respect to $x$, the order of the derivatives with respect to $x$ is reduced by two, but at the cost of the negative work of the boundary forces when the shape functions violate the dynamic boundary conditions. However, these cancel out with the work of the boundary forces, thus yielding,

$$\int_0^l \left( \left(EJ_\infty w^*_{,xx} + E_1A_1z_1\Delta u^*_{1,x}\right)\Phi_{i,xx} + N^*\left(w^*_{,x} + \hat{w}_{,x}\right)\Phi_{i,x} + \left(\mu\ddot{w}^* - p\right)\Phi_i \right) dx = 0\ , \quad i = 1,\dots,J \tag{58}$$

The evaluation of the integrals yields $J$ ordinary nonlinear coupled differential equations in $Y_i(t)$, $i = 1,\dots,J$, which are solved for $Y_i(t)$ by numerical standard solvers.

## 5. Application

### 5.1. Soft-hinged supported symmetrically layered three-layer beam

As a first application example, a symmetrically layered three-layer beam with interlayer slip is considered, whose response is governed by the equations of motion specified in Section 3.3. The soft-hinged support requires the satisfaction of the boundary conditions Eqs. (25), (26), (42), (43) and (44). The eigenfunctions of the associated linear beam with straight member axis, which are sinusoidal functions [14], are used as shape functions for the Ritz approach Eq. (56),

$$\Phi_i(x) = \sin(\lambda_i x)\ , \qquad \lambda_i = \frac{i\pi}{l}\ , \qquad i = 1,\dots,J \tag{59}$$

With these shape functions, the Ritz approach not only satisfies the kinematic boundary conditions in $w$ Eq. (25) but also the dynamic boundary conditions according to Eq. (42). The small initial deflection of the beam is also represented as a sum of sine functions,

$$\hat{w}(x) = \sum_{i=1}^{J} \hat{w}_0^{(i)} \sin(\lambda_i x) \tag{60}$$

where however the corresponding amplitudes $\hat{w}_0^{(i)}$ of the series elements are known quantities.

As explained in Section 4, the Ritz approach Eq. (56) is inserted into Eqs. (38), (39) and (37), which are then solved in combination with the remaining boundary conditions Eqs. (42), (26) and (43) for $\Delta u_1$, $\Delta u_2$ and $u^{(\infty)}$, and are now also a function of the generalized coordinates $Y_i(t)$, $i = 1,\dots,J$,

$$\Delta u^*_1(x,t) = \sum_{i=1}^{J} Y_i(t)\lambda_i^2\left(\frac{d\lambda_i\cos(\lambda_i x)}{\lambda_i^2 + \frac{K_{s1}}{E_1A_1}} - \frac{1}{4}\beta(x)\left(Y_i(t) + 2\hat{w}_0^{(i)}\right)\right) \tag{61}$$

$$\Delta u^*_2(x,t) = \sum_{i=1}^{J} Y_i(t)\lambda_i^2\left(\frac{d\lambda_i\cos(\lambda_i x)}{\lambda_i^2 + \frac{K_{s1}}{E_1A_1}} + \frac{1}{4}\beta(x)\left(Y_i(t) + 2\hat{w}_0^{(i)}\right)\right) \tag{62}$$

$$u^{(\infty)*}(x,t) = -\frac{1}{4}\sum_{i=1}^{J}\sum_{j=1}^{J}\lambda_i\lambda_j\left(\frac{1}{\lambda_{j-i}+\delta_{ji}}\sin\left(\lambda_{j-i}x\right)+\frac{1}{\lambda_{i+j}}\sin\left(\lambda_{i+j}x\right)\right)$$
$$\cdot\left(Y_i(t)Y_j(t)+Y_i(t)\hat{w}_0^{(j)}+Y_j(t)\hat{w}_0^{(i)}\right)$$
$$+\frac{\theta(x)}{4}\sum_{i=1}^{J}\lambda_i^2Y_i(t)\left(Y_i(t)+2\hat{w}_0^{(i)}\right) \tag{63}$$

with

$$\beta(x) = \frac{EA_e l\sinh\left(\frac{1}{2}\kappa\left(l-2x\right)\right)}{4E_1A_1\sinh\left(\frac{\kappa l}{2}\right)+E_2A_2\kappa l\cosh\left(\frac{\kappa l}{2}\right)},$$
$$\theta(x) = \frac{2E_1A_1\left((l-2x)\sinh\left(\frac{\kappa l}{2}\right)-l\sinh\left(\frac{1}{2}\kappa\left(l-2x\right)\right)\right)}{4E_1A_1\sinh\left(\frac{\kappa l}{2}\right)+E_2A_2\kappa l\cosh\left(\frac{\kappa l}{2}\right)} \tag{64}$$

and $\delta_{ik}$ denotes the Kronecker delta. Substituting the expressions $w^*$, $\Delta u_1^*$ and $\Delta u_2^*$ into Eq. (41) leads to the normal force as a function of $Y_i(t)$,

$$N^*(t) = \frac{\psi}{4}\sum_{i=1}^{J}Y_i(t)\lambda_i^2\left(Y_i(t)+2\hat{w}_0^{(i)}\right),$$
$$\psi = \frac{EA_eE_2A_2\kappa l\cosh\left(\frac{\kappa l}{2}\right)}{4E_1A_1\sinh\left(\frac{\kappa l}{2}\right)+E_2A_2\kappa l\cosh\left(\frac{\kappa l}{2}\right)} \tag{65}$$

By applying the Galerkin method Eq. (58), eventually the $J$ coupled ordinary differential equations for the time-dependent generalized coordinates are obtained,

$$\ddot{Y}_i+\frac{\psi\lambda_i^2}{4\mu}\left(Y_i+\hat{w}_0^{(i)}\right)\sum_{j=1}^{J}\lambda_j^2Y_j\left(Y_j+2\hat{w}_0^{(j)}\right)+\bar{\omega}_i^2Y_i=\frac{2}{\mu l}P_i\ ,\quad i=1,\dots,J \tag{66}$$

where $\bar{\omega}_i$ denotes the $i$th natural angular frequency of the corresponding linear beam with interlayer slip and straight member axis [14,15],

$$\bar{\omega}_i = \left(\frac{1}{\mu}\lambda_i^4\left(\lambda_i^2+\alpha^2\right)\left(\frac{\alpha^2}{EJ_\infty}+\frac{\lambda_i^2}{EJ_0}\right)^{-1}\right)^{1/2},\quad i=1,2,3,\dots \tag{67}$$

$$\alpha = \left(\frac{EJ_\infty K_{s1}}{E_1A_1EJ_0}\right)^{1/2} \tag{68}$$

and

$$P_i(t) = \int_0^l \Phi_i(x)p(x,t)dx\ ,\quad i=1,\dots,J \tag{69}$$

The second term of Eqs. (66) combines the quadratic and cubic nonlinearities of the present problem. The quadratic nonlinearities are solely due to the initial deflection, which disappear when the initial deflection is zero.

If these nonlinear terms are omitted, the remaining equations describe the vibration response of the slightly curved beam with interlayer slip in the linear case, i.e., for small amplitude vibrations. As can be seen, for a general initial deflection, the equations are also coupled in the linear case. However, if the initial deflection is proportional to a series member of the Ritz approach Eq. (59) (sinusoidal function): $\hat{w}(x)\sim\Phi_i(x)$, then the linear coupling elements disappear, and Eqs. (66) degenerate to a set of modal equations. Therefore, for moderately large vibrations of the considered slightly curved three-layer beams, where the initial deflection is proportional to a sinusoidal function,

$$\hat{w}(x) = \hat{w}_0^{(k)}\Phi_k(x)\ ,\quad k\in\mathbb{N}^+ \tag{70}$$

Eqs. (66) become

$$\ddot{Y}_i+\frac{\psi\lambda_i^2}{4\mu}\left(\left(Y_i+\hat{w}_0^{(k)}\delta_{ik}\right)\sum_{j=1}^{J}\lambda_j^2Y_j^2+2\lambda_k^2Y_iY_k\hat{w}_0^{(k)}\right)+\omega_i^2Y_i=\frac{2}{\mu l}P_i\ ,$$
$$i=1,\dots,J \tag{71}$$

which are coupled only through the nonlinear terms, and

$$\omega_i = \left(\frac{1}{\mu}\lambda_i^4\left(\lambda_i^2+\alpha^2\right)\left(\frac{\alpha^2}{EJ_\infty}+\frac{\lambda_i^2}{EJ_0}\right)^{-1}+\frac{1}{2\mu}\psi\lambda_k^4\left(\hat{w}_0^{(k)}\right)^2\delta_{ik}\right)^{1/2} \tag{72}$$

is the $i$th natural angular frequency of the soft hinged supported sinusoidally slightly curved three-layer beam with interlayer slip. Since there are no linear coupling terms in these equations, in an engineering approximation, damping can be accounted for by simply adding damping "modally" [32],

$$\ddot{Y}_i+\frac{\psi\lambda_i^2}{4\mu}\left(\left(Y_i+\hat{w}_0^{(k)}\delta_{ik}\right)\sum_{j=1}^{J}\lambda_j^2Y_j^2+2\lambda_k^2Y_iY_k\hat{w}_0^{(k)}\right)+2\zeta_1\omega_i\dot{Y}_i+\omega_i^2Y_i$$
$$=\frac{2}{\mu l}P_i\ ,\quad i=1,\dots,J \tag{73}$$

*Example problems.* As a first application example, the dynamic response of a three-layer beam with rectangular cross-section with layer thicknesses $h_1 = h_3 = 0.01$ m, $h_2 = 0.0102$ m, width $b = 0.1$ m and span $l = 1.0$ m is analyzed. The initial deflection against the positive $z$-coordinate in the form of a sine half-wave, $\hat{w}(x) = \hat{w}_0^{(1)}\sin(\lambda_1 x)$ (Eq. (60)), has an amplitude of 1 cm ($\hat{w}_0^{(1)} = -0.01$ m), i.e. 1% of the span $l$. The Young's modulus of the top and bottom layers is $E_1 = E_3 = 7.0\cdot10^{10}$ N/m$^2$, seven times that of the central layer $E_2 = 1.0\cdot10^{10}$ N/m$^2$. The slip modulus is $K_{s1} = K_{s2} = 1.0\cdot10^9$ N/m$^2$. Thus, the product of the layer interaction parameter $\alpha$ given by Eq. (68) and the span $l$ is $\alpha l = 13.3$, which corresponds to a moderate interaction of the layers [3]. The density of the top layers is $\rho_1 = \rho_3 = 2700$ kg/m$^3$ and of the middle layer $\rho_2 = 1000$ kg/m$^3$. The member is excited to vibration by a time-harmonic load that is half-sine wave distributed over the span $l$, applied to the beam at rest at time $t = 0$,

$$p(x,t) = p_0\sin\left(\frac{\pi x}{l}\right)\sin(\nu t) \tag{74}$$

The excitation angular frequency $\nu$ is 1.1 times the fundamental angular frequency $\omega_1$ of the corresponding linear beam with the same initial deflection, i.e. $\nu = 1.1\omega_1$, and a loading amplitude of $p_0 = 4.0\cdot10^3$ N/m is chosen.

Since the distribution of load over the beam length is proportional to the first member of the Ritz approach, only the first generalized load $P_1$ is non-zero according to Eq. (69),

$$P_1 = \frac{p_0 l}{2}\sin(\nu t) \tag{75}$$

while all other generalized loads are zero, i.e. $P_i = 0\ \forall\ i>1$. Therefore, only the first generalized coordinate $Y_1$ is included for the response analysis, and Eq. (71) becomes

$$\ddot{Y}_1+\frac{\psi\lambda_1^4}{4\mu}\left(Y_1^3+3Y_1^2\hat{w}_0^{(1)}\right)+2\zeta_1\omega_1\dot{Y}_1+\omega_1^2Y_1=\frac{2}{\mu l}P_1 \tag{76}$$

The other generalized coordinates $Y_i\ \forall\ i>1$ are not excited. Accordingly, the discretized system has one degree of freedom. Evaluating (72) yields the fundamental frequency of the corresponding linear slightly curved beam as $\omega_1 = 431.96$ rad/s.

Prior to a more detailed numerical study, the result of the proposed beam theory is compared with the outcome of a more sophisticated finite element (FE) analysis based on the assumption of a plane stress state. The FE analysis performed with the software suite Abaqus v. 2016 [35] does not need the Euler–Bernoulli hypothesis and is therefore of higher accuracy than the beam theory. In the FE model, two very thin cohesive zones with a thickness of 0.1 mm (i.e. $h_1/100$) represent the two interlayers. To ensure that the total height of the member is the same as the beam, the height of the middle layer is reduced by the thickness of the two cohesive zones (i.e. $h_2 = 0.01$ m). The cohesive zones are discretized with linear cohesive elements having four nodes per element. The tangential stiffness of these elements corresponds to the slip modulus $K_{s1}$, the normal stiffness is set $10,000K_{s1}$ as this quantity is infinite in the beam model. Quadrilateral plane

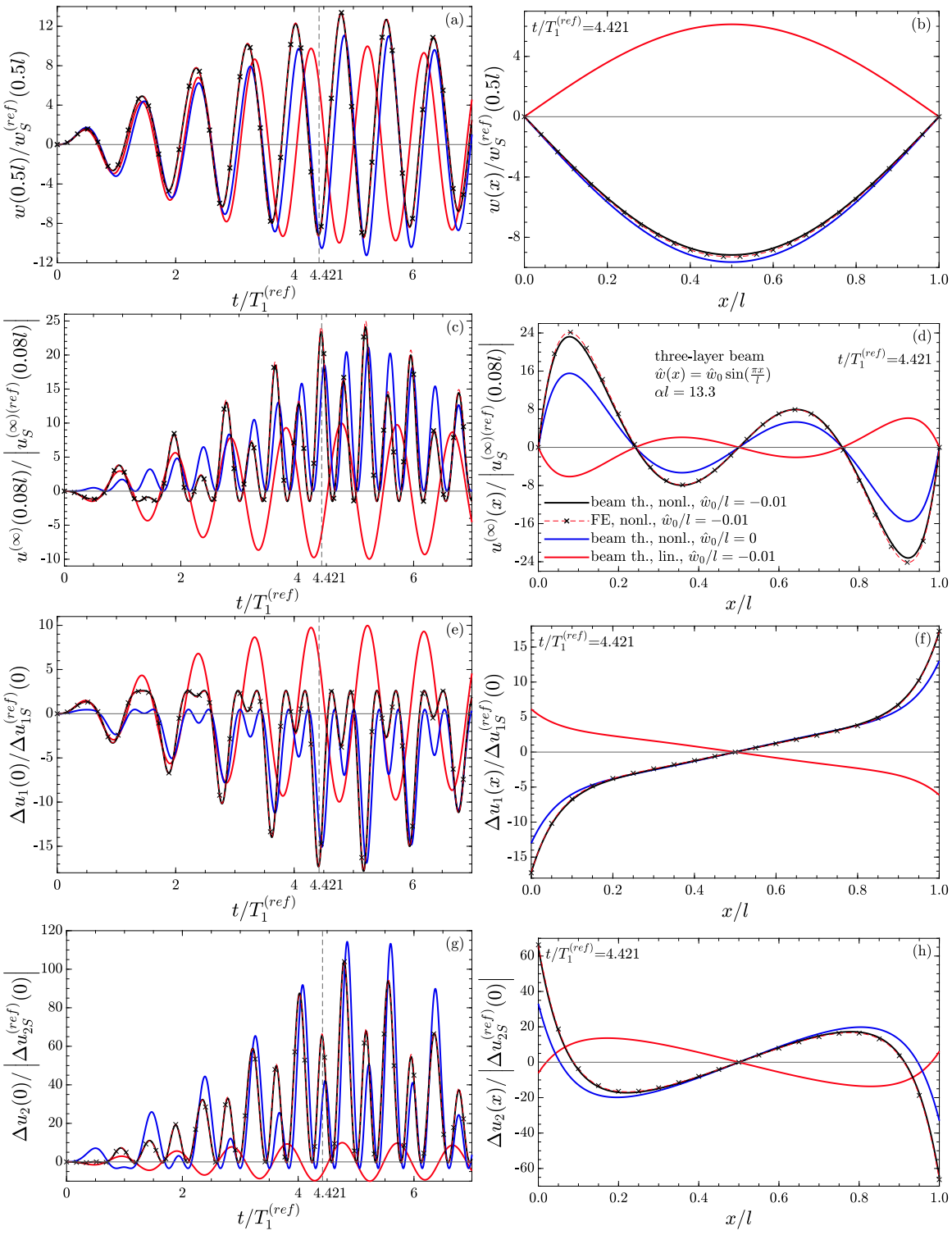


**Fig. 4.** Time history of the normalized kinematic variables at specified location (left column) and their distribution along the beam axis at a given time instant (right column): (a,b) deflection, (c,d) longitudinal displacement of the central axis, (e,f) upper interlayer slip, (g,h) lower interlayer slip. Three-layer beam.

continuum elements with eight nodes are used for the three layers. The soft-hinged supports are simulated in the FE model by means of a kinematic coupling of the outer surfaces of the central layer at an additional node. The FE model has 48,118 degrees of freedom, which is a multiple of the $J = 1$ degree of freedom of the beam theory presented. For the examination of the beam theory, the undamped beam is considered, i.e. $\zeta_1 = 0$. The computation time of the FE analysis was about 175.5 min, compared to less than 2 s to find the solution of the presented beam theory (i.e. Eq. (76)) in Mathematica v. 12.3.1 [36] on the same computer with an 8-core Intel Xeon W processor.

The left column of Fig. 4 shows the kinematic variables $w(x = 0.5l)$, $u^{(\infty)}(x = 0.08l)$, $\Delta u_1(x = 0)$, and $\Delta u_2(x = 0)$ as a function of the non-dimensional time $t/T_1^{(ref)}$, where $T_1^{(ref)} = 2\pi/\omega_1$ is the fundamental period of the corresponding linear slightly curved beam. The right column shows the distribution of these response variables along the span at time $t/T_1^{(ref)} = 4.421$. These kinematic variables have been plotted in

non-dimensional form by dividing by the corresponding reference solution. In this example, the static response quantities of the geometrically linear slightly curved beam due to loading $p_0 \sin\left(\frac{\pi x}{l}\right)$ were chosen as the reference solution (denoted by the superscript "$(ref)$" and subscript "$S$"). The non-dimensional geometrically nonlinear deflection of the slightly curved beam at midspan depicted in Fig. 4(a) with a black solid line, as a result of the beam theory presented, shows the typical beat phenomenon when excited harmonically close to a natural frequency. Its maximum value in the considered time window is reached at $t/T_1 = 4.79$. Moreover, this figure illustrates that the nonlinear deflection from the beam theory and from the FE analysis (dashed red line with markers) are virtually identical. This excellent agreement is confirmed by the plot Fig. 4(b), which shows at $t/T_1 = 4.421$ the distribution of the normalized deflection over the beam length. Comparison with the deflection of the geometrically nonlinear beam with straight beam axis ($\hat{w}_0 = 0$) (blue solid line) illustrates the influence of the small initial deflection of $\hat{w}_0 = 1\%$ of the beam length on the response. In addition, the geometrically linear response of the slightly curved beam (i.e. the geometric nonlinearities are neglected in the analysis) is also shown with a solid red line, proving how essential it is to consider the geometrically nonlinear terms in the analysis.

Also the non-dimensional longitudinal displacement of the central axis $u^{(\infty)(ref)}/u_s^{(\infty)}$ (Fig. 4(c,d)) as well as the non-dimensional upper interlayer slip $\Delta u_1/\Delta u_1^{(ref)}$ and lower interlayer slip $\Delta u_2/\Delta u_2^{(ref)}$ (Fig. 4(e,f,g,h)) confirm for this example the accuracy of the presented nonlinear beam theory compared to the higher order FE solution, and illustrate once again the importance of taking into account the initial deflection in the context of a geometrically nonlinear theory. The difference of the lower interlayer slip from the geometrically nonlinear (black solid line) and the geometrically linear (solid red line) beam theory is particularly large. While in the geometrically nonlinear case the maximum value of $\Delta u_2/\Delta u_2^{(ref)}$ at the left support ($x = 0$) in the observation period is about 110, in the geometrically linear slightly curved member it is about 10. This clearly demonstrates that the linear beam theory cannot estimate this response variable neither qualitatively nor quantitatively.

Fig. 5 shows selected internal forces for this example problem. In particular, Fig. 5(a) shows the overall normal force $N$ of the slightly curved geometrically nonlinear beam, the geometrically nonlinear beam with straight axis, and the slightly curved linear beam, divided by the overall normal force $N_S^{(ref)}$ of geometrically linear beam with initial deflection under static load. While only tension is induced in the straight beam throughout the considered time window, the normal force also assumes a negative sign in the slightly curved geometrically nonlinear beam. However, the amplitudes of the compressive normal force are less than 10% of the maximum tensile normal force. To the right, Fig. 5(b) shows the distribution of the overall normal force $N/N_S^{(ref)}$ as well as the layerwise normal forces $N_1(0.5l)/N_S^{(ref)}$, $N_2(0.5l)/N_S^{(ref)}$ and $N_3(0.5l)/N_S^{(ref)}$ of the geometrically nonlinear beam with initial deflection over the span $l$ at time $t/T_1 = 4.421$. It can be seen that at the two supports, the overall normal force is transferred into the middle layer, which is redistributed to the two outer layers in the interior of the beam. In Fig. 5(c), the time history of the overall normalized moment $M(0.5l)/M_S^{(ref)}(0.5l)$ in the beam center is also shown for the three cases described above. Fig. 5(d) depicts the distribution of the overall moment $M(0.5l)/M_S^{(ref)}(0.5l)$ as well as the layerwise bending moments $M_1(0.5l)/M_S^{(ref)}(0.5l)$, $M_2(0.5l)/M_S^{(ref)}(0.5l)$ and $M_3(0.5l)/M_S^{(ref)}(0.5l)$ of the slightly curved geometrically nonlinear beam over the span $l$ at the considered time instant.

After the validation of the beam theory in the first example problem, the influence of the initial deflection on the response of the considered beam with interlayer slip is examined from a more global perspective. To this end, in the range of the fundamental frequency, the frequency response functions of this beam with different initial deflection amplitudes is computed for $\hat{w}_0$ equal to $0, -0.01, -0.02$ and $-0.03$, respectively. That is, the initial deflection varies between 0 and 3% of the span. In contrast to the previous example, modal damping with $\zeta_1 = 5\%$ is taken into account. All other parameters as well as the load remain unchanged. To determine the frequency response functions, the beam is excited with a certain excitation frequency $\nu$ until the steady state is reached. Afterwards a new simulation is performed with a stepwise change in excitation frequency, using the modal displacement and modal velocity of the last time step of the previous simulation as initial conditions. Eventually, the response amplitude of the steady state is plotted as a function of the excitation frequency $\nu$. In the case that two different stable response amplitudes exist for one excitation frequency, a first analysis with successively incrementally increased excitation frequency (to determine the upper stable response branch) and a second analysis with successively incrementally decreased excitation frequency (to determine the smaller stable response branch) is performed.

Fig. 6(a) shows the frequency response functions of the deflection $w$ at $x = l/2$ for the beam with the four different initial deflections. The excitation frequency $\nu$ is normalized with the fundamental frequency of the linear beam with the initial deflection amplitude of $\hat{w}_0/l = -0.01$ (referred to as $\omega_1^{(ref)}$), the maximum deflection is normalized with the linear static deflection $w_S^{(ref)}$ of this member due to the load $p_0 \sin\left(\frac{\pi x}{l}\right)$. The first striking feature is the clear influence of the small initial deflection on the fundamental frequency of the corresponding linear beam, which increases with increasing initial curvature. As a result, the maximum response shifts to the right. Furthermore, it can be seen that the straight beam as well as the beam with the initial deflection of $\hat{w}_0/l = -0.01$ show a stiffening response, i.e. the amplitude frequency response "bends" to the right. In these two cases, three solutions exist in the region of the response maximum at each frequency, of which the two stable branches are shown. Another characteristic feature of the nonlinear response is the influence of the subharmonic at $\nu = \omega_1/2$ by a local maximum in the frequency response function. This influence is most pronounced for the beam with $\hat{w}_0/l = -0.01$. With increasing initial curvature, the response changes from a stiffening system to a softening system. The latter is characterized by a "slope" of the frequency response function to the left. As the effective stiffness of the beam increases with increasing $\hat{w}_0/l$, the geometrically nonlinear static deflection (i.e. $\nu/\omega_1^{(ref)} = 0$) decreases simultaneously. In contrast, however, in the present problem the maximum dynamic deflection occurs in the beam with the initial deflection $\hat{w}_0/l = -0.01$ and not in the straight beam.

The other plots in Fig. 6 show the normalized frequency response functions for the longitudinal displacement of the beam axis $u^{(\infty)}/u_S^{(\infty)(ref)}$ at $x = 0.08l$, as well as for the upper and lower interlayer slip $\Delta u_1/\Delta u_{1S}^{(ref)}$ and $\Delta u_2/\Delta u_{2S}^{(ref)}$, respectively, at the left support. The same kinematic variables of the statically loaded corresponding geometrically linear beam with the initial curvature amplitude $\hat{w}_0/l = -0.01$ serve as reference variables for the normalization. It is remarkable that for the lower interlayer slip the dynamic amplification is much larger (up to 60 for the case with $\hat{w}_0/l = -0.01$) than for the other kinematic variables.

Next, the effect of load amplitude $p_0$ on the vibration response of the beam with an initial deflection of $\hat{w}_0/l = -0.01$ is investigated. In addition to the reference load of $p_0 = p_{ref} = 4000$ N/m, the amplitude frequency responses are derived for loads $p_0 = 2p_{ref}$, $p_0 = 0.5p_{ref}$, and $p_0 = 0.25p_{ref}$. The steady state response amplitudes (e.g. the deflection $\max|w(0.5l)|$ due to $p_0 = 0.5p_{ref}$) are normalized with the corresponding linear static response of the member (i.e., the nonlinearities are neglected) due to the same load amplitude (here the deflection $w_S^{(ref,i)}(0.5l)$ due to $p_0 = 0.5p_{ref}$). Fig. 7 shows these frequency response functions for the four kinematic variables considered. For smallest load of $p_0 = 0.25p_{ref}$, the nonlinear deflection shown in Fig. 7(a) deviates only slightly from the linear deflection plotted with a dotted line.

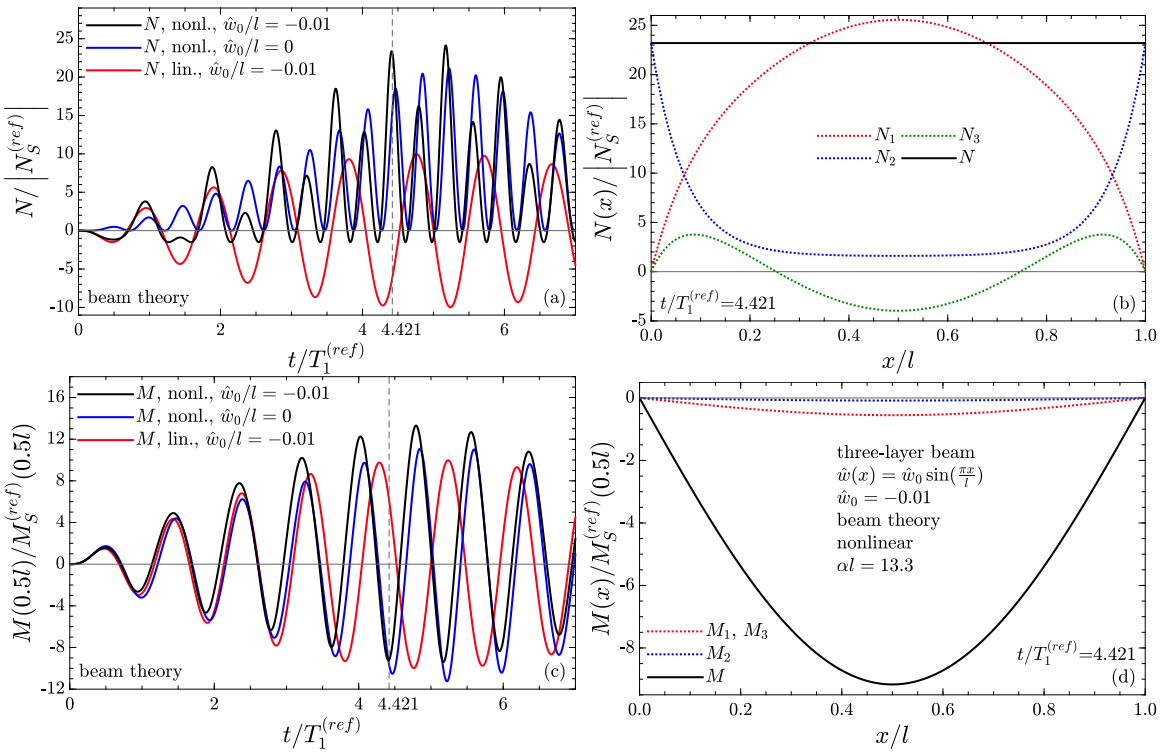


**Fig. 5.** Time history of the normalized internal forces (left) and their distribution along the beam axis at a given time instant (right). (a,b) axial forces, (c,d) bending moments. Three-layer beam.

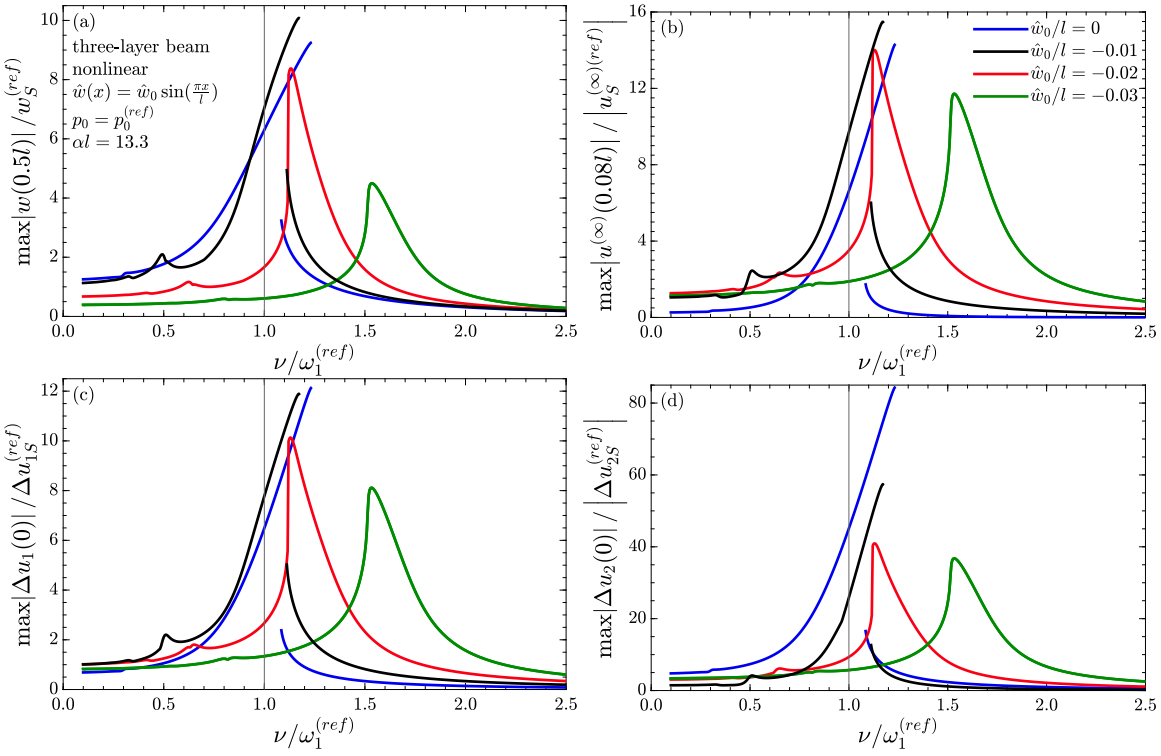


**Fig. 6.** Frequency response function of the normalized (a) deflection at midspan, (b) longitudinal displacement at $x = 0.08l$, (c) upper interlayer slip at $x = 0$, (d) lower interlayer slip at $x = 0$. Variation of the initial deflection. Three-layer beam.

That is, the maximum value of the frequency response function with a nonlinear analysis is about 10% larger than with a linear analysis. As expected, with increasing load amplitude, the nonlinearities have an increasing influence on the maximum deflection. While the maximum value of the frequency deflection function for the largest load $p_0 = 2p_{ref}$ is smaller than for the other loads, this maximum value for the three other normalized kinematic variables $u^{(\infty)}(0.08l)/u_S^{(\infty)(ref,i)}(0.08l)$, $\Delta u_1(0)/\Delta u_{1S}^{(ref,i)}(0)$ and $\Delta u_2(0)/\Delta u_{2S}^{(ref,i)}(0)$ is observed at the largest load

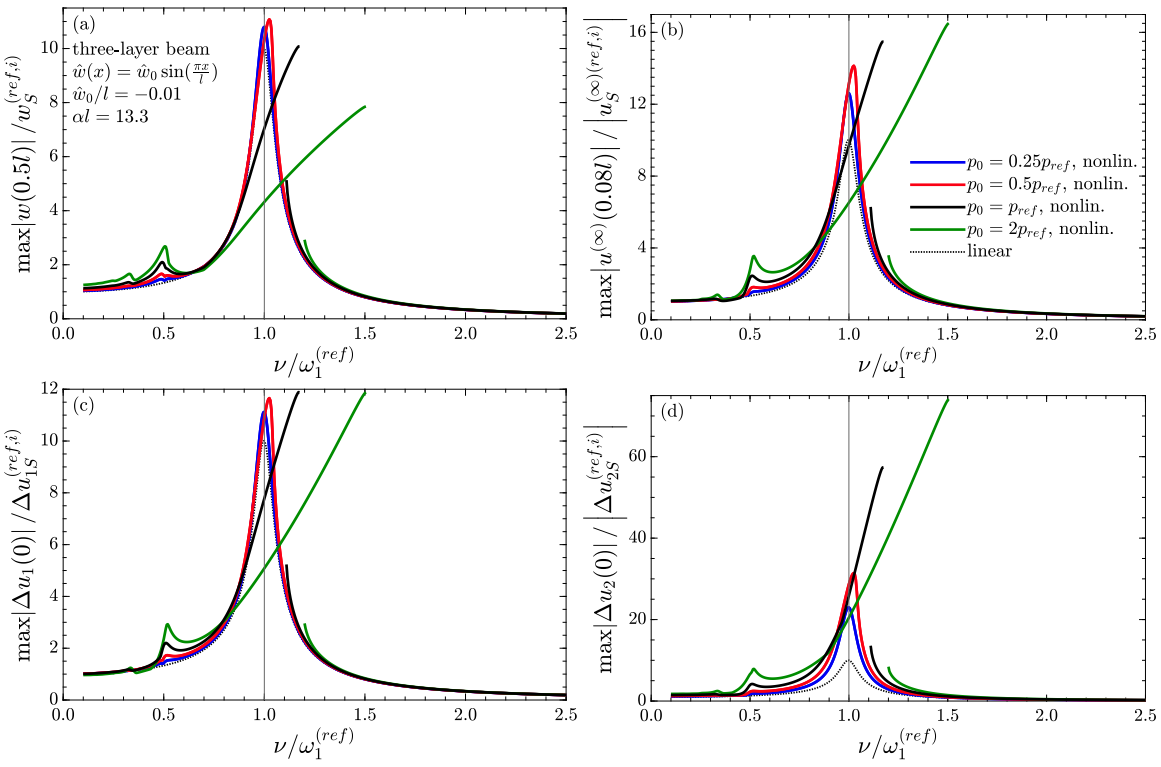


**Fig. 7.** Frequency response function of the normalized (a) deflection at midspan, (b) longitudinal displacement at $x = 0.08l$, (c) upper interlayer slip at $x = 0$, (d) lower interlayer slip at $x = 0$. Variation of the load amplitude. Three-layer beam.

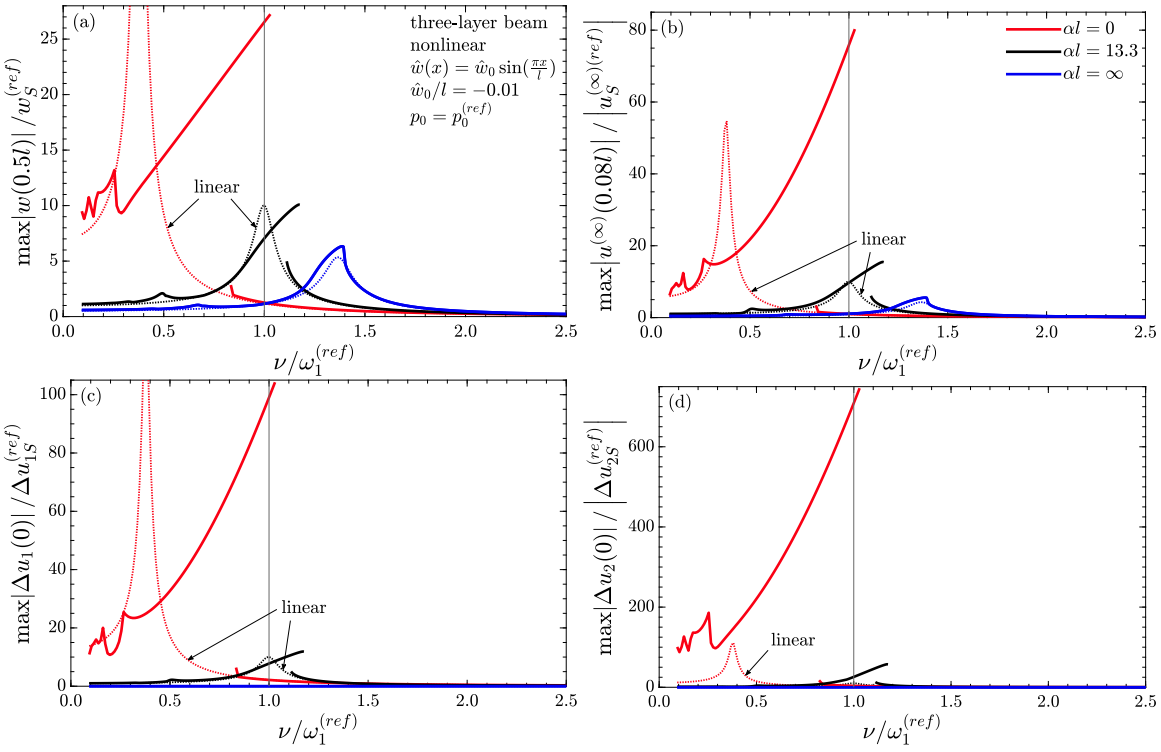


**Fig. 8.** Frequency response function of the normalized (a) deflection at midspan, (b) longitudinal displacement at $x = 0.08l$, (c) upper interlayer slip at $x = 0$, (d) lower interlayer slip at $x = 0$. Variation of the interlayer stiffness. Three-layer beam.

$p_0 = 2p_{ref}$, as shown in Fig. 7(b,c,d). The influence of the load amplitude on $\Delta u_2(0)/\Delta u_{2S}^{(ref,i)}(0)$ is particularly large, c.f. Fig. 7(d). Here, for $p_0 = p_{ref}$ the maximum dynamic magnification is about 74, while in the linear case it is only about 10.

Finally, the influence of stiffness of the interlayer bonding on the beam with the initial deflection of $\hat{w}_0/l = -0.01$ subjected the reference load of $p_0 = p_{ref}$ is investigated. In Fig. 8 the frequency response functions of the beam with slip modulus of $K_{s1} = K_{s2} = 1.0 \cdot 10^9$ N/m$^2$

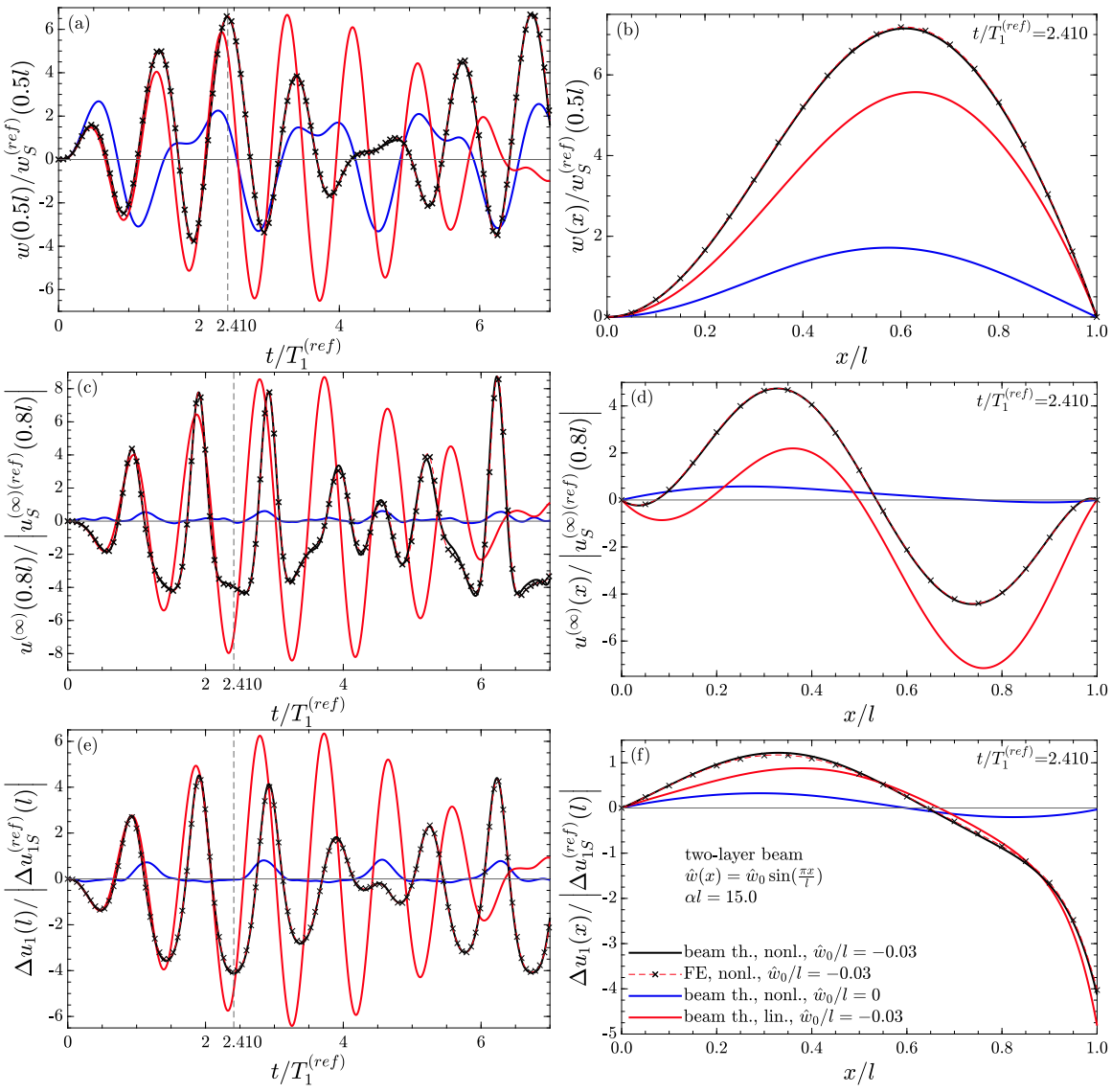


**Fig. 9.** Time history of the normalized kinematic variables at specified location (left column) and their distribution along the beam axis at a given time instant (right column): (a,b) deflection, (c,d) longitudinal displacement of the central axis, (e,f) interlayer slip. Two-layer beam.

($\alpha l = 13.3$) is compared with those of the beam with infinite slip modulus ($\alpha l = \infty$) and with those of the beam without connection of the two layers ($\alpha l = 0$). For normalization, the linear static response of the beam with $\alpha l = 13.3$ is used for three beams in this example. The graphs of this figure impressively show the effect of the interlayer bonding on the fundamental frequency, which shifts to the left as interlayer stiffness increases, and on the nonlinear dynamic response, which increases as the slip modulus decreases. The interlayer slip is clearly zero at infinite interlayer stiffness, see Fig. 8(c,d).

### *5.2. Two-layer beam clamped at the left end and soft-hinged supported at the right end*

In contrast to the three-layer symmetrically laminated beam, for the two-layer beam on a soft-hinged support the dynamic boundary conditions of the geometrically linear beam and the geometrically nonlinear beam are different. While in the case of the geometrically nonlinear beam the deflection $w$ and the interlayer slip $\Delta u_1$ are coupled at the support through Eqs. (53) and (54), these two quantities are decoupled in the linear case (i.e., $(w_{,xx})_b = (\Delta u_{1,x})_b = 0$). Consequently, if the eigenfunctions of the linear beam were used as shape functions in the Ritz approach Eq. (56) for the analysis of the nonlinear response of the slightly curved nonlinear beam, the boundary conditions Eqs. (53) and (54) cannot be satisfied. Therefore, for the asymmetrically layered beam, polynomials $\boldsymbol{\Phi}_j(x)$ are used as shape functions in the Ritz approach Eq. (56) [37],

$$w(x,t) \approx w^*(x,t) = \sum_{i=i_a}^{J} Y_i(t)\boldsymbol{\Phi}_i(x)\ , \quad \boldsymbol{\Phi}_i(x) = \left(\frac{x}{l}\right)^i \left(1-\frac{x}{l}\right)^{i_b} \tag{77}$$

The lower value of the sum $i_a$ depends on the geometric boundary conditions in the deflection $w$ that must be satisfied at $x = 0$, and the exponent $i_b$ depends on the geometric boundary conditions $w$ that must be satisfied at $x = l$, as follows [37],

soft-hinged support, hard-hinged support at $x = 0 : i_a = 1$

at $x = l : i_b = 1$ (78)

clamped end at $x = 0 : i_a = 2$

at $x = l : i_b = 2$ (79)

With a beam clamped at $x = 0$, the two geometric boundary conditions $w(0) = w_{,x}(0) = 0$ must be satisfied, and thus $i_a = 2$. With a hinged support at $x = 0$ with $w(0) = 0$, $i_a = 1$. For the sake of completeness, it

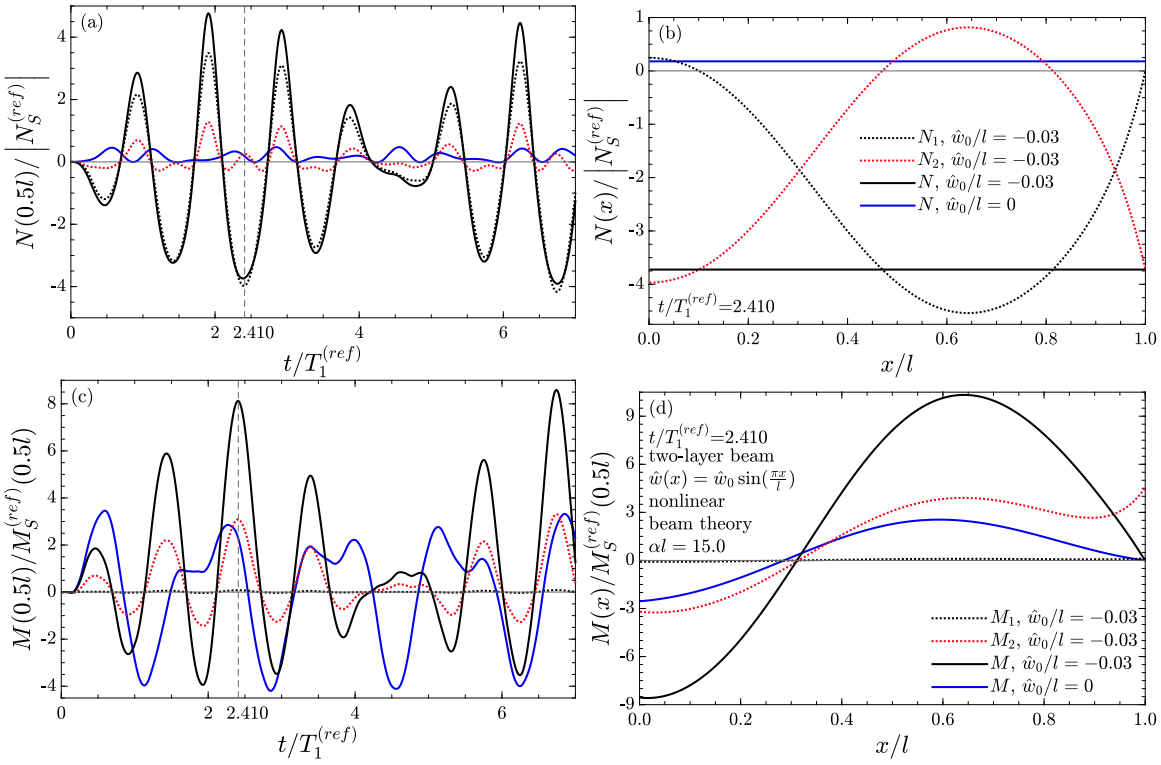


**Fig. 10.** Time history of the normalized internal forces (left) and their distribution along the beam axis at a given time instant (right). (a,b) axial forces, (c,d) bending moments. Two-layer beam.

should be mentioned that for a free end the parameters would have to be chosen as follows: $x=0:\ i_a=0$; $x=l:\ i_b=0$. However, a free end is not considered here for reasons already discussed.

Now the procedure described in Section 4 can be applied. Solving the Eqs. (49) and (50) in combination with the actual boundary conditions specified in Section 3.4 with the Ritz approach Eq. (77) employed yields analytical expressions for $\Delta u_1$ and $u^{(\infty)}$ (now denoted as $\Delta u_1^*(x,t)$ and $u^{(\infty)*}(x,t)$) as a function of the generalized coordinates $Y_i(t)$, $i=i_a,\dots,J$, with linear, quadratic and mixed quadratic dependence. Subsequent $J-i_a+1$ times evaluation of Galerkin's rule Eq. (58) leads to a set of $J-i_a+1$ ordinary nonlinear coupled differential equations for the generalized coordinates $Y_i(t)$ with linear, quadratic, mixed-quadratic, cubic, and mixed-cubic dependencies. This set of nonlinear generalized vibration equations is solved numerically, and inserting the obtained $Y_i(t)$ in $w^*(x,t)$, $\Delta u_1^*(x,t)$ and $u^{(\infty)*}(x,t)$ leads to the approximation of the vibration response of the beam problem at hand. It should be noted here that as the number of $J-i_a+1$ series members in Eq. (77) increases not only the accuracy of the kinematic response but also the dynamic boundary conditions are better approximated. The analytical and numerical computations described here were performed for the subsequently presented example problem with the software package Mathematica [36].

*Example problem.* The considered two-layer beam with rectangular cross-section and length $l=1.0$ m is clamped on the left end and soft-hinged immovably supported on the right end. The upper layer with dimensions $h_1=0.004$ m and $b_1=0.1$ m has Young's modulus $E_1=7.0\cdot10^10$ N/m$^2$ and density $\rho_1=2700$ kg/m$^3$, for the lower layer with dimensions $h_2=0.026$ m and $b_2=0.1$ m, these quantities are $E_2=1.0\cdot10^{10}$ N/m$^2$ and $\rho_2=1000$ kg/m$^3$. The interlayer stiffness is $K_{s1}=1.0\cdot10^9$ N/m$^2$. Thus, the layer interaction parameter $\alpha$ for the two-layer beam [3],

$$\alpha=\left(K_{s1}\left(\frac{EA_e}{E_1A_1E_2A_2}+\frac{(h_1/2+h_2/2)^2}{EJ_0}\right)\right)^{1/2} \tag{80}$$

times span $l$ is $\alpha l=15.0$. The beam is slightly curved against the positive $z$-direction according to a half-sine wave with amplitude $\hat{w}_0/l=-0.03$, i.e. 3% of the span. Its fundamental frequency is $\omega_1=841.4$ rad/s. At time $t=0$ a time-harmonic load equally distributed over the beam is applied: $p(x,t)=p_0\sin(\nu t)$. The load amplitude is $p_0=6000$ N/m, the excitation frequency $\nu$ 1.15 times the fundamental frequency: $\nu=1.15\omega_1$. For predicting the vibration response with the presented beam theory, $J=9$ shape functions are used; this number was found to be appropriate by a convergence study.

To validate the nonlinear beam theory, the response of this member is also determined with an FE analysis in Abaqus v. 2016 [35] based on a plane stress state. As for the example of the three-layer beam presented earlier, in the FE model the interlayer is discretized by cohesive elements with thickness 0.0001 m. Thus, the height of the lower layer $h_2$ is reduced by this amount (i.e., $h_2=0.026$ m) to keep the total height of the beam the same. For further details compare with the description of the three-layer beam example. The FE model has approximately 34,910 degrees of freedom, in contrast to the beam model with 8 degrees of freedom (since $J=9$ and $i_a=2$). Also in this example, the computation time for the beam solution was orders of magnitude faster than for the FE analysis.

In the following figures the response is again shown non-dimensionally. For normalization, the corresponding static response variable of the geometrically linear slightly curved beam subjected to the load $p=p_0$ is used. In the left column of Fig. 9, non-dimensional deflection at beam center, longitudinal displacement of the central axis at location $x/l=0.8$, and interlayer slip at the right end of the beam are shown as a function of dimensionless time $t/T_1^{(ref)}$, where $T_1^{(ref)}=2\pi/\omega_1$ denotes the fundamental period of the slightly curved beam. At time $t/T_1^{(ref)}=2.410$, the right column displays the distribution of these kinematic response quantities along the beam axis $x/l$. The comparison of the solution of the presented beam theory illustrated with a black line with the FE solution (dashed line with markers) proves again the accuracy of the beam theory. In

the considered time window, the deviation between these solutions is negligible. The response shown with a red solid line is the result of a linear analysis of the curved beam, i.e., the nonlinearities were neglected. The difference between the nonlinear and linear solution is considerable and demonstrates the importance of the nonlinear terms for the estimation of the vibration response. Last but not least, the nonlinear response of the beam with straight beam axis (i.e., $\hat{w}_0 = 0$) is also shown with a blue solid line, whose shape, magnitude and distribution over $x/l$ differs substantially from that of the slightly curved beam.

Fig. 10 shows the overall $N/N_S^{(ref)}$ and layerwise partial normal forces $N_1(0.5l)/N_S^{(ref)}$, $N_2(0.5l)/N_S^{(ref)}$ (upper row) as well as overall $M(l/2)/M_S^{(ref)}(l/2)$ and layerwise partial bending moments $M_1(0.5l)/M_S^{(ref)}(l/2)$, $M_2(0.5l)/M_S^{(ref)}(l/2)$ (lower row) of the nonlinear slightly curved beam. In addition, the overall normal force and the overall bending moment are depicted with a blue solid line for the beam with straight member axis, which are quite different from the results of the slightly curved beam. These results illustrate once more the importance of considering the initial deflection for the computational estimation of the internal forces. According to Fig. 10(b), at the hinged support (right end), the total normal force is equal to the normal force in the lower layer (i.e., $N = N_2(l)$). At the same support, the total moment is zero, $M(l) = 0$, however, as can be also observed from the boundary conditions Eqs. (54) and (53), the bending moment in the lower layer $M_2$ is not zero. This means that with the 9 shape functions the dynamic boundary conditions are virtually identically satisfied.

## 6. Conclusions

In this contribution, a novel beam theory for the prediction of the nonlinear moderately large vibration response of slightly curved layered beams with interlayer slip was presented. This theory is based on a layerwise application of the Euler–Bernoulli theory and a linear slip law. A semianalytic solution was found for the symmetrically layered three-layer beam with both ends immovably soft-hinged supported. For more general beam configurations, a numerical solution procedure was presented, which was applied to the example of a two-layer beam. Comparison of the vibration response found with this beam theory with results obtained from finite element analyses assuming a plane stress state showed excellent agreement. Moreover, the effect of geometric nonlinearity, initial deflection and interlayer slip on the moderately large vibration response was revealed. Since the beam theory is computationally much more efficient than the finite element analysis, it is very suitable to search for benchmark solutions.

## CRediT authorship contribution statement

**Christoph Adam:** Conceptualization, Methodology, Formal analysis, Resources, Supervision, Investigation, Writing – original draft. **Dominik Ladurner:** Methodology, Software, Validation, Formal analysis, Visualization, Investigation, Writing – review & editing. **Thomas Furtmüller:** Methodology, Supervision, Writing – review & editing.

## Declaration of competing interest

The authors declare that they have no known competing financial interests or personal relationships that could have appeared to influence the work reported in this paper.

## Data availability

The data that has been used is confidential.

## References


[1] Goodman JR, Popov EP. Layered beam systems with interlayer slip. J Struct Div 1968;94:2535–48.

[2] Girhammar UA, Gopu VKA. Composite beam-columns with interlayer slip-exact analysis. J Struct Eng 1993;119:1265–82.

[3] Girhammar UA, Pan DH. Exact static analysis of partially composite beams and beam-columns. Int J Mech Sci 2007;49(2):239–55. http://dx.doi.org/10.1016/j.ijmecsci.2006.07.005, URL http://www.sciencedirect.com/science/article/pii/S0020740306001512.

[4] Gahleitner J, Schoeftner J. A two-layer beam model with interlayer slip based on two-dimensional elasticity. Compos Struct 2021;274:114283. http://dx.doi.org/10.1016/j.compstruct.2021.114283, URL https://www.sciencedirect.com/science/article/pii/S0263822321007455.

[5] Lezgy-Nazargah M, Vidal P, Polit O. A sinus shear deformation model for static analysis of composite steel-concrete beams and twin-girder decks including shear lag and interfacial slip effects. Thin-Walled Struct 2019;134:61–70. http://dx.doi.org/10.1016/j.tws.2018.10.001, URL https://www.sciencedirect.com/science/article/pii/S0263823118300569.

[6] Ecsedi I, Lengyel AJ. Curved composite beam with interlayer slip loaded by radial load. Curved Layer Struct 2015;2(1):25–40.

[7] Kryžanowski A, Schnabl S, Turk G, Planinc I. Exact slip-buckling analysis of two-layer composite columns. Int J Solids Struct 2009;46(14):2929–38. http://dx.doi.org/10.1016/j.ijsolstr.2009.03.020, URL http://www.sciencedirect.com/science/article/pii/S0020768309001450.

[8] Simon S, Miran S, Goran T, Igor P. Analytical solution of two-layer beam taking into account interlayer slip and shear deformation. J Struct Eng 2007;113:886–94.

[9] Challamel N. On geometrically exact post-buckling of composite columns with interlayer slip—The partially composite elastica. Int J Non-Linear Mech 2012;47(3):7–17. http://dx.doi.org/10.1016/j.ijnonlinmec.2012.01.001, URL https://www.sciencedirect.com/science/article/pii/S0020746212000029.

[10] Ranzi G, Bradford M. Analytical solutions for the time-dependent behaviour of composite beams with partial interaction. Int J Solids Struct 2006;43(13):3770–93. http://dx.doi.org/10.1016/j.ijsolstr.2005.03.032, URL https://www.sciencedirect.com/science/article/pii/S0020768305001447.

[11] Mistakis ES, Thomopoulos K, Avdelas A, Panagiotopoulos PD. On the nonmonotone slip effect in the shear connectors of composite beams. Int J Eng Anal Des 1994;1:395–409.

[12] Uddin MA, Sheikh AH, Brown D, Bennett T, Uy B. A higher order model for inelastic response of composite beams with interfacial slip using a dissipation based arc-length method. Eng Struct 2017;139:120–34. http://dx.doi.org/10.1016/j.engstruct.2017.02.025, URL https://www.sciencedirect.com/science/article/pii/S0141029616309816.

[13] Monetto I. Analytical solutions of three-layer beams with interlayer slip and step-wise linear interface law. Compos Struct 2015;120:543–51. http://dx.doi.org/10.1016/j.compstruct.2014.09.003, URL https://www.sciencedirect.com/science/article/pii/S026382231400436X.

[14] Girhammar UA, Pan D. Dynamic analysis of composite members with interlayer slip. Int J Solids Struct 1993;30:797–823.

[15] Adam C, Heuer R, Jeschko A. Flexural vibrations of elastic composite beams with interlayer slip. Acta Mech 1997;125:17–30.

[16] Heuer R. Thermo-piezoelectric flexural vibrations of viscoelastic panel-type laminates with interlayer slip. Acta Mech 2006;181(3):129–38. http://dx.doi.org/10.1007/s00707-005-0299-y.

[17] Girhammar UA, Pan DH, Gustafsson A. Exact dynamic analysis of composite beams with partial interaction. Int J Mech Sci 2009;51(8):565–82. http://dx.doi.org/10.1016/j.ijmecsci.2009.06.004, URL https://www.sciencedirect.com/science/article/pii/S0020740309001052.

[18] Challamel N, Bernard F, Casandjian C. Out-of-plane behaviour of partially composite or sandwich beams by exact and finite element methods. Thin-Walled Struct 2010;48(8):561–80. http://dx.doi.org/10.1016/j.tws.2010.03.005, URL https://www.sciencedirect.com/science/article/pii/S0263823110000510.

[19] Nguyen Q-H, Hjiaj M, Le Grognec P. Analytical approach for free vibration analysis of two-layer timoshenko beams with interlayer slip. J Sound Vib 2012;331(12):2949–61. http://dx.doi.org/10.1016/j.jsv.2012.01.034, URL https://www.sciencedirect.com/science/article/pii/S0022460X12001058.

[20] Lorenzo SD, Adam C, Burlon A, Failla G, Pirrotta A. Flexural vibrations of discontinuous layered elastically bonded beams. Composites B 2018;135:175–88. http://dx.doi.org/10.1016/j.compositesb.2017.09.059, URL http://www.sciencedirect.com/science/article/pii/S1359836817316657.

[21] Lee J. Free vibration analysis of delaminated composite beams. Comput Struct 2000;74(2):121–9. http://dx.doi.org/10.1016/S0045-7949(99)00029-2, URL https://www.sciencedirect.com/science/article/pii/S0045794999000292.

[22] Krawczyk P, Rebora B. Large deflections of laminated beams with interlayer slips. 2007;24(1):33–51. http://dx.doi.org/10.1108/02644400710718565.

[23] Kim H-J, Yoon K, Lee P-S. Continuum mechanics based beam elements for linear and nonlinear analyses of multi-layered composite beams with interlayer slips. Compos Struct 2020;235:111740. http://dx.doi.org/10.1016/j.compstruct.2019.111740, URL https://www.sciencedirect.com/science/article/pii/S0263822319309110.

[24] Battini J-M, Nguyen Q-H, Hjiaj M. Non-linear finite element analysis of composite beams with interlayer slips. Comput Struct 2009;87(13):904–12. http://dx.doi.org/10.1016/j.compstruc.2009.04.002, URL https://www.sciencedirect.com/science/article/pii/S0045794909000790.

[25] Ranzi G, Dall'Asta A, Ragni L, Zona A. A geometric nonlinear model for composite beams with partial interaction. Eng Struct 2010;32(5):1384–96. http://dx.doi.org/10.1016/j.engstruct.2010.01.017, URL https://www.sciencedirect.com/science/article/pii/S0141029610000180.

[26] Tseng WY, Dugundji J. Nonlinear vibrations of a beam under harmonic excitation. J Appl Mech 1970;37(2):292–7, URL http://dx.doi.org/10.1115/1.3408504.

[27] Elishakoff I, Birman V, Singer J. Influence of initial imperfections on nonlinear free vibration of elastic bars. Acta Mech 1985;55(3):191–202. http://dx.doi.org/10.1007/BF01175801, URL https://doi.org/10.1007/BF01175801.

[28] Tseng J. Nonlinear vibrations of a buckled beam under harmonic excitation. J Appl Mech 1971;38(2):467–76.

[29] Adam C. Moderately large vibrations of imperfect elastic-plastic composite beams with thick layers. Int J Acoust Vib 2002;7(1):11–20.

[30] Adam C, Ladurner D, Furtmüller T. Moderately large deflection of slightly curved layered beams with interlayer slip. Arch Appl Mech 2022. http://dx.doi.org/10.1007/s00419-022-02119-z.

[31] Adam C, Furtmüller T. Moderately large deflections of composite beams with interlayer slip. In: Altenbach H, Irschik H, Matveenko VP, editors. Contributions to advanced dynamics and continuum mechanics. Cham: Springer International Publishing; 2019, p. 1–17. http://dx.doi.org/10.1007/978-3-030-21251-3{_}1.

[32] Adam C, Furtmüller T. Flexural vibrations of geometrically nonlinear composite beams with interlayer slip. Acta Mech 2020;231(1):251–71. http://dx.doi.org/10.1007/s00707-019-02528-2.

[33] Mettler E. In: Flügge W, editor. Dynamic buckling. New York: McGraw-Hill; 1962, 62–1–62–11.

[34] Ziegler F. Mechanics of solids and fluids. 2nd ed.. Springer New York; 1995.

[35] Abaqus FEA v. 2016. Simulia (Dassault Systèmes); 2021.

[36] Mathematica v. 11.2.0. Wolfram Research, Inc.; 2017.

[37] Qatu M. In-plane vibration of slightly curved laminated composite beams. J Sound Vib 1992;159(2):327–38. http://dx.doi.org/10.1016/0022-460X(92)90039-Z, URL https://www.sciencedirect.com/science/article/pii/0022460X9290039Z.